ELSEVIER

Journal of Non-Crystalline Solids 303 (2002) 270–280

JOURNAL OF NON-CRYSTALLINE SOLIDS

www.elsevier.com/locate/jnoncrysol

Dependence of nanocrystalline SnO_2 particle size on synthesis route

Mira Ristić [a,*], Mile Ivanda [a], Stanko Popović [b], Svetozar Musić [a]

[a] *Division of Materials Chemistry, Ruđer Bošković Institute, P.O. Box 180, 10002 Zagreb, Croatia*
[b] *Department of Physics, University of Zagreb, P.O. Box 331, 10002 Zagreb, Croatia*

Received 19 March 2001; received in revised form 5 September 2001

Abstract

Very fine SnO_2 powders were produced by (a) slow and (b) forced hydrolysis of aqueous $SnCl_4$ solutions and (c) hydrolysis of tin(IV)-isopropoxide dissolved in isopropanol (sol–gel route) and then characterized by X-ray powder diffraction, Fourier transform infrared and laser Raman spectroscopies, TEM and BET. The XRD patterns showed the presence of the cassiterite structure. As found from XRD line broadening the crystallite sizes of all powders were in the nanometric range. TEM results also showed that the sizes of SnO_2 particles in all powders are in nanometric range. Very fine SnO_2 powders showed different features in the FT-IR spectra, depending on the route of their synthesis. The reference Raman spectrum of SnO_2 showed four bands at 773, 630, 472 and 86 (shoulder) cm^{-1}, as predicted by group theory. Very fine SnO_2 powders showed additional Raman bands, in dependence on their synthesis. The broad Raman band at 571 cm^{-1} was ascribed to amorphous tin(IV)-hydrous oxide. The additional Raman bands at 500, 435 and 327 cm^{-1} were recorded for nanosized SnO_2 particles produced by forced hydrolysis of $SnCl_4$ solutions. However, these additional Raman bands were not observed for nanosized SnO_2 particles produced by slow hydrolysis of $SnCl_4$ solution or the sol–gel route. The aggregation effects of nanosized particles were considered in the interpretation of the Raman band at 327 cm^{-1}. The method of low frequency Raman scattering was applied for SnO_2 particle size determination. On the basis of these measurements it was concluded that the size of SnO_2 particles was also in the nanometric range and that, the sol–gel particles heated to 400 °C consisted of several SnO_2 crystallites. © 2002 Published by Elsevier Science B.V.

1. Introduction

Tin dioxide, SnO_2, and SnO_2-based ceramics found various applications as gas sensors, catalysts, electrode materials, etc. The properties of these oxides, such as particle size and morphology, structural and physical properties and crystallinity, greatly depend on the route of their synthesis. It is, therefore, understandable that in the past many researchers tried to correlate the experimental parameters of SnO_2 synthesis with the properties of this compound. For example, spherical and rod-like SnO_2 particles were produced by heating $SnCl_4$ solution at 100 °C in the presence of urea or formamide [1]. The change in the morphology of the SnO_2 particles from spherical to rod-like was correlated to the pH of the suspension. Spherical

* Corresponding author. Tel.: +385-1 46 80 107; fax: +385-1 46 80 098.
E-mail address: ristic@rudjer.irb.hr (M. Ristić).

0022-3093/02/$ - see front matter © 2002 Published by Elsevier Science B.V.
PII: S0022-3093(02)00944-4

SnO_2 particles of submicrometer dimensions were also produced by the hydrolysis of $SnCl_4$ aerosol droplets with NH_3 gas [2].

Hydrous SnO_2 gels were produced by adding concentrated NH_4OH solution into aqueous $SnCl_4$ solution at pH 1, 5 or 11 at room temperature [3]. The amount of residual chloride ions affected the sol/gel equilibria in this colloidal system. At higher concentrations of residual chloride ions the gelation process was retarded. SnO_2 was also produced by forced hydrolysis of 0.01 M aqueous $SnCl_4$ solution and additional heating of the isolated precipitate between 300 and 900 °C [4]. For this temperature range the size of crystallites was 3.9–62.1 nm, as determined by the broadening of XRD lines. Hydrous SnO_2 was precipitated from aqueous $SnCl_4$ solution using decomposing urea as generator of OH^- ions [5]. The thus produced tin(IV)-hydrous oxide contained 75 wt% of water. When sulphate ions were added to the precipitation system, the size of the spherical particles of SnO_2 was 0.14 ± 0.03 μm and they contained 13.5 wt% of water.

The pyrolysis method was used for the preparation of SnO_2 films, as well as SnO_2 powders. SnO_2 films were deposited on hot alumina substrates by this method [6]. The texture of the films varied from dense to porous after heating in the 450–600 °C temperature range. The pyrolysis temperature for SnO_2 films for the application in gas detection, should be higher to obtain porous films with a maximum specific surface area. On the other hand, SnO_2 films characterized with good optical transparency required high density of the material, implying lower pyrolysis temperatures. Spherical SnO_2 particles were also produced from $SnCl_4$ aqueous solution using ultrasonic spray pyrolysis [7]. The mean diameter of SnO_2 particles increased with the concentration of $SnCl_4$ solution from 0.2 to 0.8 μm. Each spherical particle consisted of many primary particles. Vallet-Regi et al. [8] produced SnO_2 particles using pyrolysis of an aerosol obtained by ultrahigh frequency spraying of a $SnCl_2$ solution in a tubular furnace. In the presence of HCl and tartarate ions, the formation of SnO_2 was found by XRD, whereas poor crystallized products were obtained from the solutions containing oxalate ions. SEM of all these samples showed that the SnO_2 particles were in the form of hollow spherical particles. The particles (3–5 nm) of platinum were codeposited on fine SnO_2 particles (8–25 nm) using ultrahigh frequency spraying [9].

In the literature several additional methods for the production of SnO_2 powders or thin films were also reported. SnO_2 powders were produced using the laser ablation method [10,11]. Very fine SnO_2 powders were produced in a DC transferred arc plasma furnace [12]. The initial agglomeration of SnO_2 particles was intensified during additional heat treatment of these particles and this was accompained by a reduction in the surface area. Optimization of the experimental parameters was achieved, eliminating the need for additional thermal treatment. Cho et al. [13] produced SnO_x thin films on Si 1 0 0 substrates using reactive ion-assisted deposition.

SnO_2 films to be applied as gas sensors were modified using implantation of gold and iron ions [14]. After ion implantation and annealing at 600 °C the sensitivity to H_2, C_2H_5OH and CO was enhanced over a wide range of gas concentrations. Enoki et al. [15] investigated the structural and electro-optical properties of vacuum-deposited indium-doped SnO_2. As this material is characterized by good electrical and optical transparency, it can be used as a transparent electrode.

In the last decade, the attention of researchers was focused on the sol–gel method for the synthesis of various metal oxides. This method can be used for the production of (a) metal oxides at relatively low processing temperatures, (b) metal-oxides free from foreign ions, (c) metal oxides with precise control of the doping level, and (d) metal oxides with the particles in the nanosize range. Many sol–gel procedures for the production of fine powders and thin films of various metal oxides were described in the literature. For example, SnO_2 thin films were prepared [16] by the sol–gel route using an alcoholic solution of $Sn(OC_2H_5)_4 \cdot 2C_2H_5OH$ as the precursor. Subsequently these films were heated and annealed between 500 and 700 °C and the sensitivity of these films to relative humidity was measured.

In the present work we investigated the formation and properties of SnO_2 particles using (a) slow

and (b) forced hydrolysis of $SnCl_4$ aqueous solutions and (c) hydrolysis of tin(IV)-isopropoxide dissolved in isopropanol (sol–gel route). The aim of this work was to ascertain the differences in the formation of SnO_2 particles using above-mentioned methods of the Sn^{4+} hydrolysis. Special attention was paid to particle size determination, using the method of low frequency Raman scattering (LFRS). These results were compared with the SnO_2 crystallite sizes determined from XRD line broadening. The LFRS method was successfully applied for the first time [17] for the size determination of nanosized metal oxide particles, which are not embeded into the host matrix, such as an oxide glass, and this method was also confirmed by subsequent investigations [18–20].

2. Experimental

Anhydrous tin(IV)-chloride, tin(IV)-isopropoxide, $Sn(OCH(CH_3)_2)_4$, 10% w/v in isopropanol, and isopropanol, were used. Doubly distilled water was used in all experiments. Spectral properties of very fine SnO_2 powders were compared with those of commercial SnO_2.

The samples were prepared using two different routes of tin(IV) hydrolysis. In the first case, 0.384 M aqueous $SnCl_4$ solution was aged for a period of 10 years at room temperature (slow hydrolysis). The precipitate formed by slow hydrolysis of $SnCl_4$ solution was isolated using a superspeed centrifuge. This precipitate was subsequently washed with doubly distilled water and then dried at 55 °C for 48 h. The precursor liquor was hydrothermally treated at 160 °C (forced hydrolysis) for different times. The samples were also produced using the sol–gel route. Tin(IV) was hydrolized by adding doubly distilled water to the solution of tin(IV)-isopropoxide in isopropanol. The precipitates produced by the sol–gel route were also dried at 55 °C for 48 h. The experimental conditions for the preparation of the samples are given in Table 1.

X-ray powder diffraction patterns were taken using an automatic diffractometer (CuKα radiation, graphite monochromator, proportional counter). The crystallite size was determined by the Scherrer method applied to diffraction lines, 1 0 1 and 1 1 0.

Table 1
Experimental conditions for the preparation of SnO_2 powders

Sample	History of sample
S1	Hydrolysis of 0.384 M $SnCl_4$ at room temperature for 10 years.
S2	Autoclaving of precursor liquor at 160 °C for 2 h.
S3	Autoclaving of precursor liquor at 160 °C for 6 h.
S4	Autoclaving of precursor liquor at 160 °C for 24 h.
S5	Precipitate S1 heated at 600 °C for 4 h.
S6	25 ml of original Sn(IV)-isopropoxide solution was diluted with 15 ml of isopropanol. 10 ml of H_2O was used for hydrolysis. Refluxed at 100 °C for 3h. pH = 5.5. Precipitate dried in a Petri dish at 55 °C for 48 h.
S7	Sample S6 heated at 400 °C for 2 h.
S8	25 ml of original Sn(IV)-isopropoxide solution was diluted with 24.5 ml of isopropanol. 0.5 ml H_2O was used for the hydrolysis at RT. pH = 5.5. Precipitate dried in a Petri dish at 55 °C for 48 h.
S9	Sample S8 heated at 400 °C for 2 h.

Fourier transform infrared spectra of the specimens pressed into KBr discs were recorded at room temperature. An IR Data Manager (IRDM) program was used to process the FT-IR spectra recorded.

Raman spectra were collected using a triple monochromator spectrometer. An Argon ion laser with $\lambda = 514.5$ nm was used as the excitation source. To avoid laser heating of the sample, the laser beam was focused as a line of 2×0.05 mm^2 in size. The laser power applied to the sample was 50 mW.

Transmission electron microscopy (TEM) was performed. For TEM characterization a small amount of powder was dispersed in doubly distilled water using an ultrasound bath. A drop of this dispersion was put onto a copper grid previously coated with a thin film of organic polymer.

The BET measurements were performed using a surface area analyzer.

3. Results

Fig. 1 shows characteristic parts of XRD patterns of the precipitate produced by hydrolysis of 0.384 M aqueous solution at RT for 10 years (sample S1) and of the precipitates produced by autoclaving the mother liquor at 160 °C over 2–24 h (samples S2–S4). In the same figure, the char-

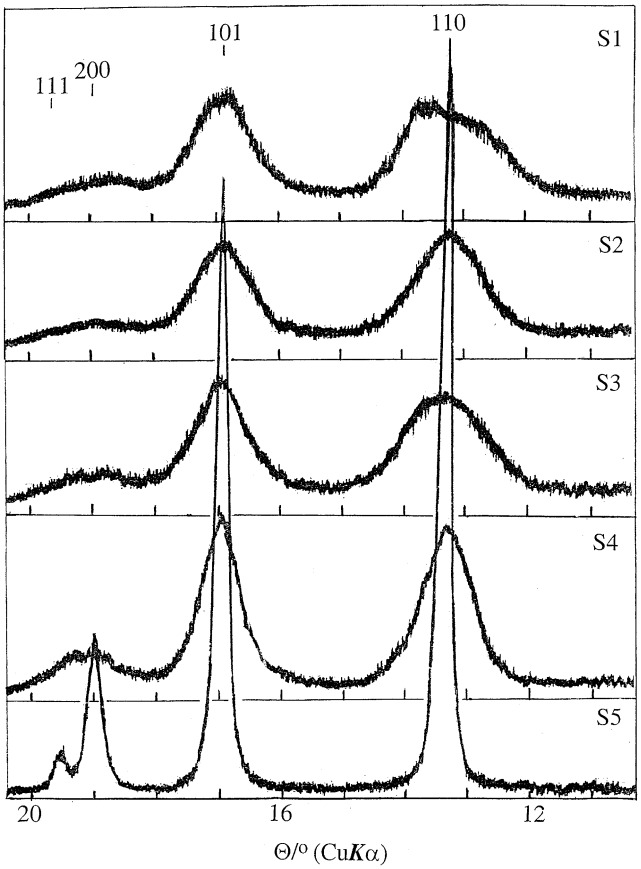

Fig. 1. Characteristic parts of XRD patterns of samples S1–S5 recorded at room temperature. S1 was produced by slow hydrolysis of a 0.384 M $SnCl_4$ solution at room temperature (RT) for 10 years. S2, S3 and S4 were produced by forced hydrolysis of the mother liquor at 160 °C for 2, 6 and 24 h, respectively. S5 was produced by heating sample S1 to 600 °C.

acteristic part of the XRD pattern of the thermal decomposition product (sample S5), obtained by heating of sample S1 at 600 °C for 4 h, indicated the diffraction lines of SnO_2 [21].

The average crystallite size D of the samples (Table 2) was calculated using the Scherrer equation:

$$D = 0.9\lambda/\beta\cos\Theta,$$

where λ is the X-ray wavelength, Θ is the Bragg angle and β is the pure full width of the diffraction line at half its maximum intensity. The crystallite sizes of the products of slow hydrolysis and forced hydrolysis at 160 °C are evidently in the nanometric range, with a tendency of a slight increase with prolonged time of autoclaving.

Table 2
Average crystallite sizes determined by XRD and particle sizes determined by LFRS of samples S1–S4 and samples S6–S9

Sample	Crystallite size (nm)[a]		Particle size (nm)
	Diffraction line 1 1 0	Diffraction line 1 0 1	
S1	–[b]	4.1	2.94
S2	3.5	4.1	3.50
S3	3.1	4.2	3.64
S4	4.6	5.9	4.31
S6	2.4	–[b]	2.05
S7	5.2	5.5	8.62
S8	Amorphous		Amorphous
S9	4.8	5.2	12.2

[a] Estimated standard deviation of the crystallite size values is about 20%.

[b] Not calculated due to overlapping of diffraction lines.

Fig. 2 shows characteristic parts of XRD patterns of samples S6–S9 produced by hydrolysis of tin(IV)-isopropoxide. Sample S6 showed very broad overlapping diffraction lines due to very small crystallite sizes. After heating sample S6 at 400 °C, the obtained sample S7 exhibited narrower, but still very broad and partially overlapping diffraction lines. This decrease of broadening indicated the growth of the crystallite size from 2.4 nm (sample S6) to 5.2 nm (sample S7), as determined from the width of diffraction line 1 1 0. The characteristic part of the XRD pattern of sample S8 showed its amorphous nature. After heating sample S8 at 400 °C, the XRD pattern of sample S9 was similar to that of sample S7. The crystallite sizes, obtained from the widths of diffraction lines 1 1 0 and 1 0 1 of sample S9 were 4.8 and 5.2 nm, respectively. In the XRD patterns of samples S7, S8 and S9 either one or two very sharp diffraction peaks of small intensities were observed. The origin of these possibly parasitic peaks was no further investigated.

The FT-IR spectra of samples S1–S4 are shown in Fig. 3. For comparison, the FT-IR spectrum of commercial SnO_2 is also shown in the same figure.

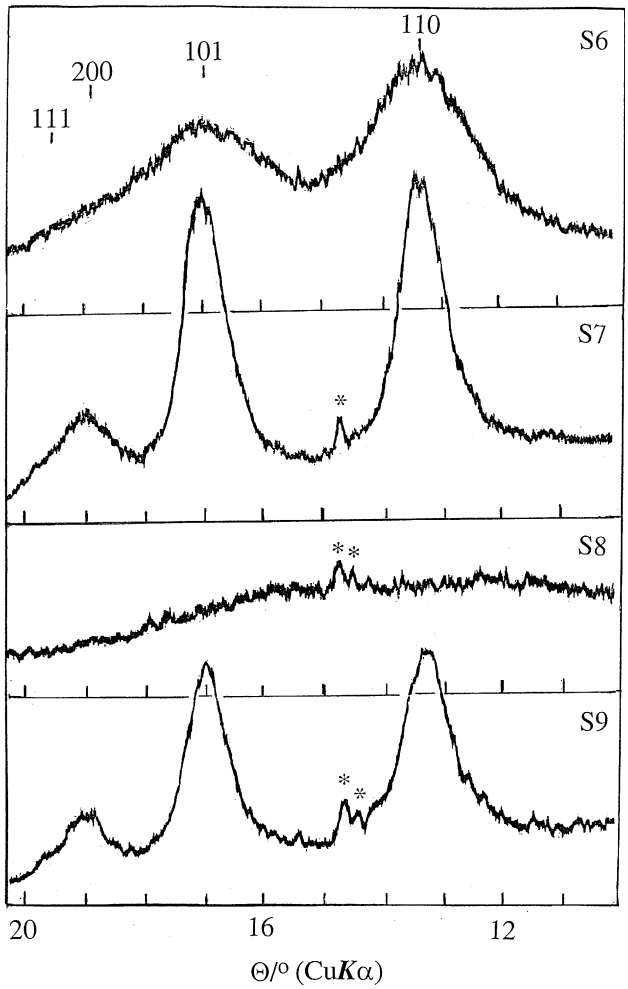

Fig. 2. Characteristic parts of XRD patterns of samples S6–S9, recorded at room temperature. S6 and S8 were produced by the sol–gel route. S6 was refluxed at 100 °C for 3 h, whereas S8 was kept at room temperature. S7 and S9 were produced after heating the corresponding samples S6 and S8 at 400 °C. (*) unidentified peaks.

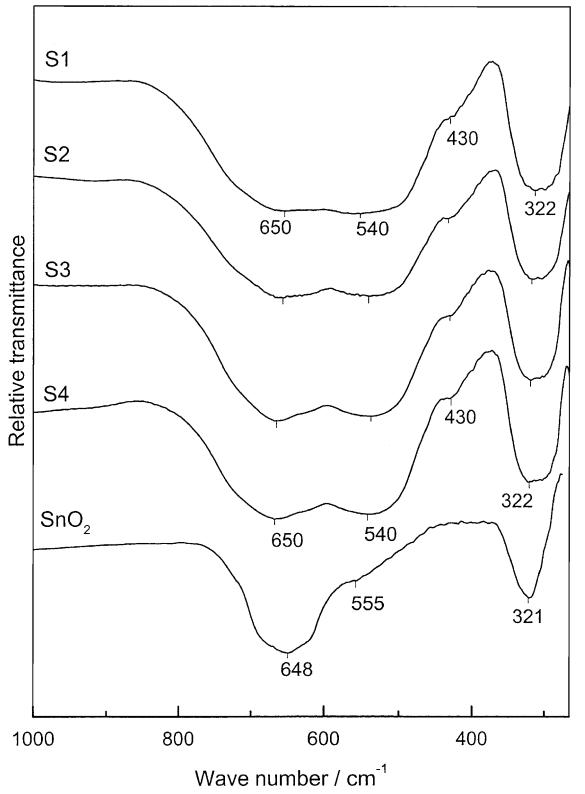

Fig. 3. Fourier transform infrared spectra of samples S1–S4, recorded at room temperature. For comparison, the FT-IR spectrum of commercial SnO_2 is also shown.

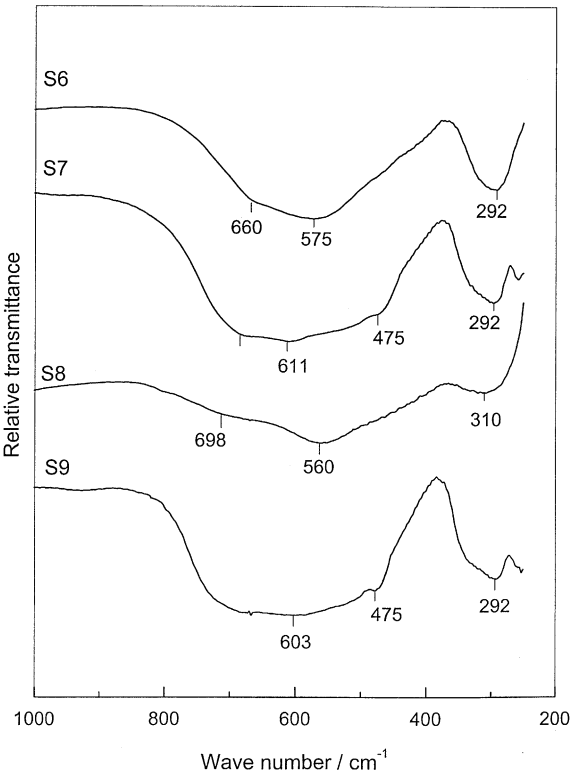

Fig. 4. Fourier transform infrared spectra of samples S6–S9, recorded at room temperature.

The FT-IR spectra of samples S1–S4 are characterized by bands at 650 and 540 cm^{-1}, shoulder at 430 cm^{-1} and the band at 322 cm^{-1}. The spectrum of commercial SnO_2 showed a very strong and broad band at 648 cm^{-1} with a shoulder at 555 cm^{-1} and a second band at 321 cm^{-1}.

Fig. 4 shows the FT-IR spectra of the samples obtained by the sol–gel route and their calcination products produced at 400 °C (samples S6–S9). The shapes of these spectra differ in relation to those recorded for the precipitates produced by hydrolysis of aqueous $SnCl_4$ solutions. Sample S6 shows the most intense band of SnO_2 at 575 cm^{-1} with a shoulder at 660 cm^{-1}. After heating sample S6 at 400 °C, a very strong and broad band centered at 611 cm^{-1} was observed. For sample S8 an IR band at 560 cm^{-1} and a shoulder at 698 cm^{-1} were recorded, and after heating sample S8 to 400 °C (sample S9), a spectrum similar to that of sample S7 was recorded.

The Raman spectra of samples S1–S4, commercial SnO_2 and samples S6–S9 are shown in Figs. 5 and 6. Raman spectrum of the commercial SnO_2 in Fig. 5 shows a pronounced band at 630 cm^{-1}, corresponding to A_{1g} mode, and two bands at 773 and 472 cm^{-1} corresponding to B_{2g} and E_g modes, respectively; this being in accordance with literature data [22,23]. In the low-frequency region a shoulder at 86 cm^{-1}, due to B_{1g} mode, is also visible. The samples prepared in the present work showed Raman bands of SnO_2. Sample S1, obtained by slow hydrolysis of aqueous $SnCl_4$ solution, showed two Raman bands of small relative intensity at 620 and 773 cm^{-1} due to SnO_2 with a rutile-type structure. A more intense and broad band at 571 cm^{-1} is ascribed to amorphous fraction of tin(IV)-hydrous oxide. These Raman results support the conclusion based on the XRD

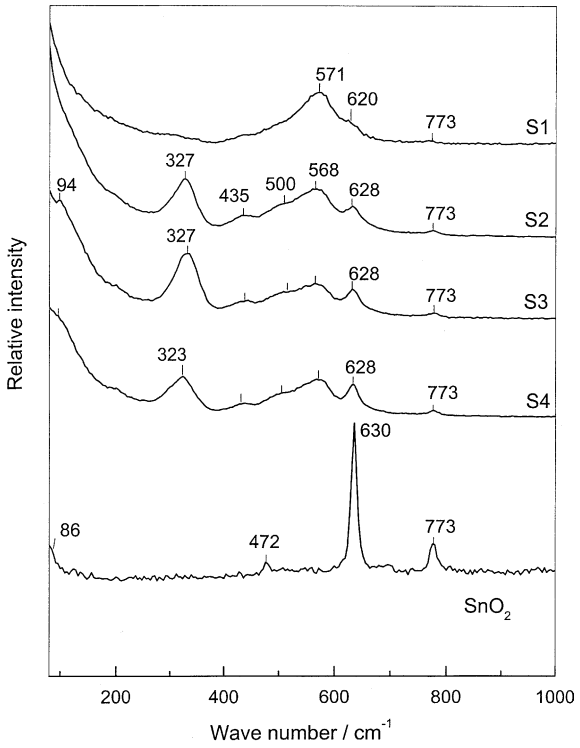

Fig. 5. Raman spectra of samples S1–S4, recorded at room temperature. For comparison, the Raman spectrum of commercial SnO_2 is also shown.

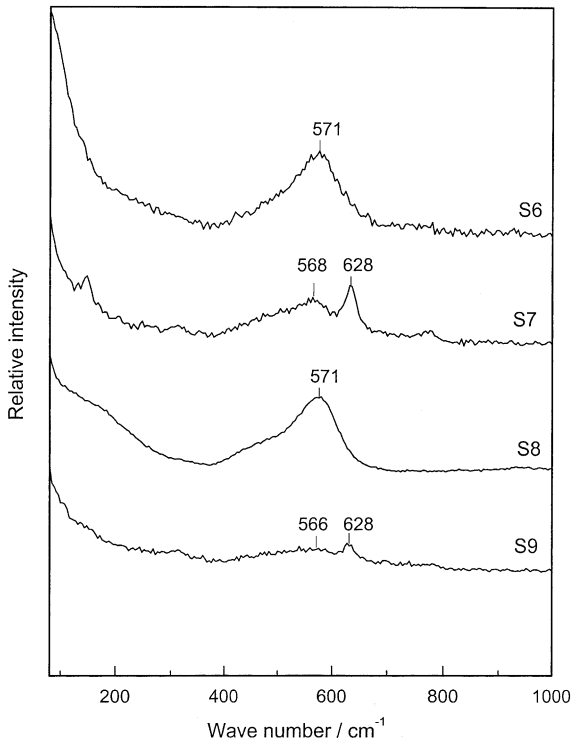

Fig. 6. Raman spectra of samples S6–S9, recorded at room temperature.

characterization of this sample. Raman spectra of samples S2, S3 and S4 obtained by forced hydrolysis of aqueous $SnCl_4$ solution showed additional bands at 500 and 435 cm^{-1}, and at 327 cm^{-1}, which are not predicted by group theory. Raman spectra of samples S6 and S8, prepared by the sol–gel route, show a very broad and intense Raman band at 571 cm^{-1}, which can be ascribed to amorphous tin(IV)-hydrous oxide. This position is in the region of the Raman band observed at 566 cm^{-1} for SnO_2 film [23].

In the present work the LFRS method [17–20] was applied to determine the size of SnO_2 particles in nanometric range. This method is based on work of Duval et al. [24], originally applied to crystallized cordierite glass in the region of low-frequency Raman scattering. The authors showed that the maximum of the low-frequency Raman band was proportional to the inverse diameter of the spherical spinel microcrystallites. Gotić et al. [17] applied the LFRS method for the first time to the size determination of nanocrystalline TiO_2 particles which were not inside any matrix. This method was successfully tested on several nanocrystalline TiO_2 samples by comparing LFRS with the complementary techniques, such as XRD, HRTEM and SAXS [19]. Theoretical background of this method was reported in previous works [25,26].

The low-frequency parts of the Raman spectra of the samples S1–S4 and S6–S9 are shown in Figs. 7 and 8. The positions of low-frequency Raman peaks used in the calculation of the particle size are denoted in these figures and the results of the calculation are given in Table 2. There is good agreement between these results and those obtained for crystallite size by the Scherrer method. It can be concluded that in the case of samples S7 and S9, produced by additional heating at 400 °C, the particle size is approximately doubled relative to the crystallite size determined by XRD. This

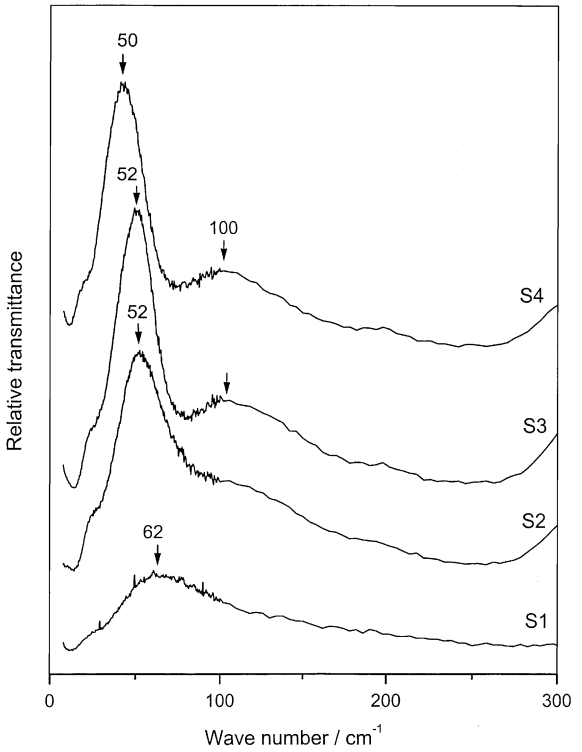

Fig. 7. Low frequency Raman spectra of samples S1–S4, recorded at room temperature.

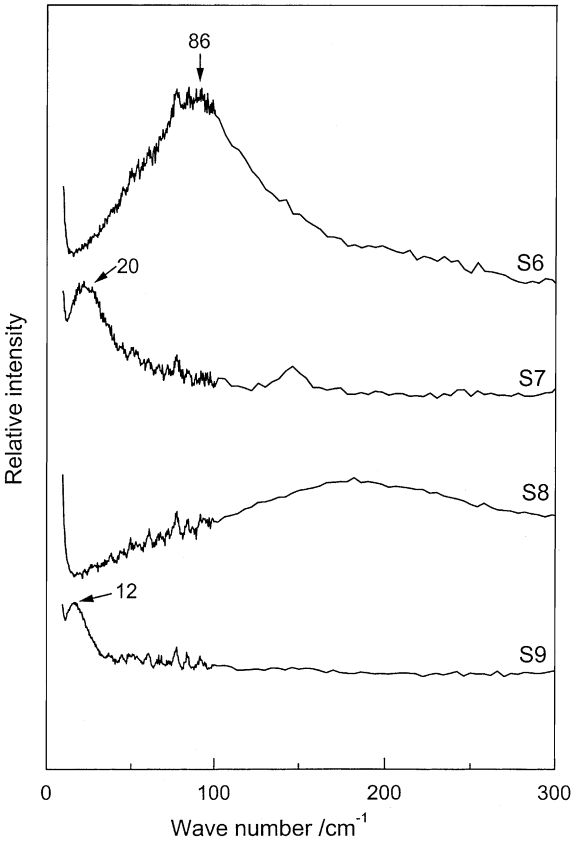

Fig. 8. Low frequency Raman spectra of samples S6–S9, recorded at room temperature.

indicates that in samples S7 and S9 the SnO_2 particles consist of a several crystallites.

Fig. 9 shows TEM photographs of samples S4, S6 and commercial SnO_2. Two kinds of aggregation for nanosized SnO_2 particles were observed. Nanosized SnO_2 particles produced by forced hydrolysis aggregated in the form of chains (Fig. 9(a)). On the other hand, in the samples produced by sol–gel route the SnO_2 particles crystallized inside the amorphous matrix. These crystallized SnO_2 particles showed discrete positions inside the amorphous matrix (big agglomerates in Fig. 9(b)). TEM photograph of commercial SnO_2 sample (Fig. 9(c)) showed much bigger and non-uniform particles.

4. Discussion

The XRD analysis of samples S1–S4, produced by the hydrolysis of $SnCl_4$ solution, showed the diffraction lines corresponding to the rutile-type structure (cassiterite) [21]. However, in the case of sample S1 the most intense diffraction line 1 1 0 typical for cassiterite can be considered as the superposition of two diffraction lines. After treatment at 600 °C for 4 h this sample showed well-developed diffraction lines of cassiterite (sample S5). A similar effect was observed by Sangaletti et al. [27] during their investigation of the oxidation of Sn thin films to SnO_2, and they suggested that in their case, the formation of SnO_x ($1.33 < x < 1.5$) was possibly a phase associated to the main phase of SnO_2. In the present case it appears that there are two distributions of the hydrolytical products in sample S1 varying in crystal ordering and stoichiometry and causing the diffraction line 1 1 0 of sample S1 to appear as a superposition of two

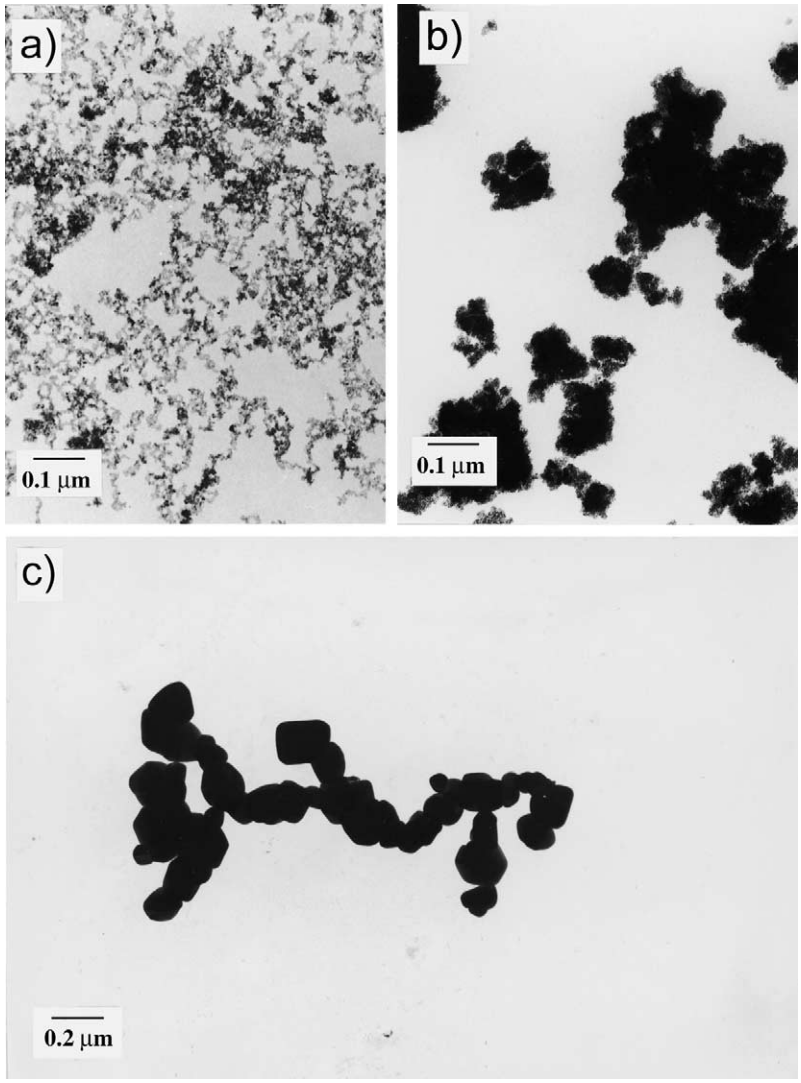

Fig. 9. TEM photographs of samples (a) S4, (b) S6 and (c) commercial SnO_2.

diffraction maxima. In the reference literature [28] there is also a hypothesis suggesting that hydroxylation and formation of oxy-bridges are preferentially processed in the planes 1 1 0. In this stage of hydrolysis various structural defects on the surface, as well as in the bulk of Sn(IV)-hydrous oxide particles, may be formed. The XRD analysis of sample S6, produced by the sol–gel route, showed very small crystallite size (2.4 nm) of the crystalline fraction in the sample, whereas the XRD pattern of sample S8 showed its amorphous nature. The XRD pattern of sample S6 also showed a significant amorphous fraction (Fig. 2).

All FT-IR spectra, shown in Figs. 3 and 4 can be related with SnO_2 in spite of differences in their spectral shape. Generally, the IR spectrum of SnO_2 with rutile-type structure was discussed by Ocaña et al. [29,30]. They showed an influence of the particle shape on the IR spectrum of SnO_2. For very fine SnO_2 crystallites ($\sim$2 nm) a very strong and broad band at 575 cm^{-1} with a shoulder at 660 cm^{-1} and a band at 300 cm^{-1} were recorded [30].

Since electron microscopy showed spherical SnO_2 particles of much greater dimensions, it was concluded that very fine SnO_2 crystallites are structural units of larger spherical particles. With an increase of the crystallite size and overall crystallinity two resolved IR bands at 650–635 and 505 cm^{-1} were recorded [30]. The additional band at 320 cm^{-1} was considered [29] to be overlapping of two E_u modes at a lower frequency, due to the presence of elongated particles and a small amount of oblate spheroids.

In the present work the FT-IR spectrum of commercial SnO_2 can be interpreted similar, as it was done by Ocaña and Serna [29]. In this sense, the shoulder at 555 cm^{-1} can be ascribed to the presence of non-uniform SnO_2 particles. This can be confirmed by TEM photograph (Fig. 9(c)) of commercial SnO_2 sample which showed non-uniform particles that are not in nanometric range. On the other hand, the IR band at 540 cm^{-1} recorded for particles S1–S4 is strongly influenced with the nanometer size of these particles and significant amorphous fraction. The presence of nanosized SnO_2 particles is confirmed by TEM (Fig. 9(a)), whereas the XRD showed significant amorphous fraction which decreased with prolonged time of forced hydrolysis. The formation of various structural defects cannot be excluded.

The samples S6 and S8 prepared by the sol–gel route showed IR bands centered at 575 and 560 cm^{-1}, respectively. For these samples XRD showed almost (sample S6) or completely (sample S8) amorphous character. After treatment of samples S6 and S8 at 400 °C a very broad bands centered at 611 and 603 cm^{-1} were observed (Fig. 4). Evidently, the shifts of IR bands $575 \rightarrow 611$ cm^{-1} and $560 \rightarrow 603$ cm^{-1} can be related with the crystallization of nanosized SnO_2 particles from amorphous material. Jiménez et al. [31] prepared SnO_2 nanocrystalline powders by the gas phase condensation method using polycrystalline SnO as the precursor material. Their SnO_2 particles also showed high amorphous fraction (~80–90%) which decreased to 20% in the sample annealed at 500 °C.

Nature of SnO_2 particles also strongly influenced the corresponding Raman spectra, as shown in Figs. 5 and 6. According to group theory, a single SnO_2 crystal with rutile-type structure shows four Raman active modes, A_{1g}, B_{1g}, B_{2g} and E_g. The additional A_{2u} and E_u modes correspond to transverse-optical (TO) and longitudinal-optical (LO) vibrations [22]. The spectrum of commercial SnO_2 sample showed the Raman bands in accordance with the theory. However, additional Raman bands, which are not predicted by group theory, are also visible in the spectra of some samples. For example, sample S1, obtained by slow hydrolysis of $SnCl_4$ solution, showed two Raman bands at 620 and 773 cm^{-1} due to SnO_2 with a rutile-type structure, whereas the dominant Raman band at 571 cm^{-1} can be ascribed to amorphous fraction of tin(IV)-hydrous oxide. Additional Raman bands at 500, 435 and 327 cm^{-1} observed for samples S2, S3 and S4, produced by forced hydrolysis of aqueous $SnCl_4$ solutions are not predicted by group theory. These additional Raman bands were observed also by other researchers [22,30], when they used hydrothermally prepared SnO_2 particles. However, in the case of slow hydrolysis (sample S1) the prominent band at 327 cm^{-1} was not observed. In order to obtain more information about the surfaces of these samples we measured the specific surface area by BET. The measured values are: 210.3 $m^2 g^{-1}$ for sample S1, 159.4 $m^2 g^{-1}$ for sample S2 and 129.8 $m^2 g^{-1}$ for sample S4, that is the logic sequence. Ocaña et al. [30] generally suggested that additional Raman bands observed for SnO_2 samples can be related to the surface defects of the particles. On the other hand Yu et al. [22] attributed the above phenomena to the microstructure of nanocrystalline SnO_2. They proposed the formation of SnO_2 nanoclusters which might constitute a new kind of vibration mode. In our case, TEM of the particles produced by forced hydrolysis (for example, sample S4 in Fig. 9(a)) showed aggregation of nanosized particles in the form of 1D chains. On the other hand, in the case of sol–gel route, nanosized SnO_2 particles crystallized inside the amorphous matrix (Fig. 9(b)) showing 3D aggregation of discrete SnO_2 particles. On the basis of these aggregation differences of nanosized SnO_2 particles the phonon mode at 327 cm^{-1} could be attributed to the confinement effect of the phonons in the 1D chains.

5. Conclusions

Very fine SnO_2 particles were produced by (a) slow and (b) forced hydrolysis of aqueous $SnCl_4$ solutions and (c) hydrolysis of tin(IV)-isopropoxide dissolved in isopropanol (sol–gel route). The XRD patterns corresponded to SnO_2 with rutile-type structure (cassiterite). Crystallite size determination based on the Scherrer method showed that all samples were in the nanometric range. FT-IR spectroscopy showed different spectral features of very fine SnO_2 powders, in dependence on the route of their synthesis. These spectral differences were related to the microstructural properties of nanosized SnO_2 particles. The Raman spectrum of commercial SnO_2, used as reference, showed four bands at 773, 630, 472 and 86 (shoulder) cm^{-1}, as predicted by group theory. However, the Raman spectra of the hydrolytical products of aqueous $SnCl_4$ solutions showed an additional Raman band at 571 cm^{-1} which can be ascribed to amorphous tin(IV)-hydrous oxide. The Raman spectra of very fine SnO_2 particles, produced by sol–gel route, showed also an amorphous peak at 571 cm^{-1}. Additional Raman bands at 500, 435 and 327 cm^{-1} were recorded for nanosized SnO_2 particles produced by forced hydrolysis of $SnCl_4$ solutions. TEM showed different aggregation of nanosized SnO_2 particles, obtained by forced hydrolysis of $SnCl_4$ solutions, in relation to the other methods of the synthesis. For this reason, the aggregation effects of nanosized SnO_2 particles were considered in the interpretation of the Raman band at 327 cm^{-1}. The method of LFRS was applied to particle size determination. There was a good agreement between SnO_2 crystallite size determination by the Scherrer method and particle size determination by LFRS. The sol–gel particles heated to 400 °C consisted of several SnO_2 crystallites.

References

[1] M. Ocaña, E. Matijević, J. Mater. Res. 5 (1990) 1083.
[2] M. Ocaña, C.J. Serna, E. Matijević, Colloid Polym. Sci. 273 (1995) 681.
[3] R.S. Hiratsuka, S.H. Pulcinelli, C.V. Santilli, J. Non-Crystall. Solids 121 (1990) 76.
[4] Q. Li, X. Yuan, G. Zeng, S. Xi, Mater. Chem. Phys. 47 (1997) 239.
[5] B.-K. Kim, I. Yasui, J. Mater. Sci. 23 (1988) 637.
[6] F. Caillaud, A. Smith, J.-F. Baumard, Thin Solid Films 208 (1992) 4.
[7] J.-H. Lee, S.-J. Park, J. Am. Ceram. Soc. 76 (1993) 777.
[8] M. Vallet-Regi, V. Ragel, J. Román, J. Martinez, M. Labeau, A. Varela, J.M. González-Calbet, Solid State Ionics 63–65 (1993) 164.
[9] M. Labeau, B. Gautheron, F. Cellier, M. Vallet-Regi, E. Garcia, J.M. González-Calbet, J. Solid State Chem. 102 (1993) 434.
[10] G. Williams, G.S.V. Coles, J. Mater. Chem. 8 (1998) 1657.
[11] M.J. Willett, V.N. Burganos, C.D. Tsakiroglou, A.C. Payatakes, Sens. Actuat. B 53 (1998) 76.
[12] F. Qafssaoui, F. Benyaich, J.-M. Baronnet, Ann. Chim. Fr. 19 (1994) 391.
[13] J.S. Cho, S.K. Song, H.-J. Jung, S.K. Koh, W.K. Choi, K.H. Yoon, J. Mater. Sci. 16 (1997) 524.
[14] K. Nomura, S. Shiozawa, T. Takada, H. Reuther, E. Richter, J. Mater. Sci.: Mater. Electron. 8 (1997) 301.
[15] H. Enoki, K. Yamamori, J. Echigoya, J. Mater. Sci. Lett. 10 (1991) 970.
[16] T.M. Racheva, G.W. Critchlow, Thin Solid Films 292 (1997) 299.
[17] M. Gotić, M. Ivanda, A. Sekulić, S. Musić, S. Popović, A. Turković, K. Furić, Mater. Lett. 28 (1996) 225.
[18] M. Gotić, M. Ivanda, S. Popović, S. Musić, A. Sekulić, A. Turković, K. Furić, J. Raman Spectr. 28 (1997) 555.
[19] A. Turković, M. Ivanda, S. Popović, A. Tonejc, M. Gotić, P. Dubček, S. Musić, J. Molec. Struct. 410&411 (1997) 271.
[20] M. Ivanda, S. Musić, S. Popović, M. Gotić, J. Molec. Struct. 480–481 (1999) 645.
[21] International Centre for Diffraction Data, Joint Committee on Powder Diffraction Standards, Powder Diffraction File, 1601 Park Lane, Swarthmore, PA 19081, USA.
[22] K.N. Yu, Y. Xiong, Y. Liu, C. Xiong, Phys. Rev. B 55 (1997) 2666.
[23] T. Asari, T. Sato, J. Phys. Soc. Jpn. 66 (1997) 1360.
[24] E. Duval, A. Boukenter, B. Champagnon, Phys. Rev. Lett. 56 (1986) 2052.
[25] M. Ivanda, S. Musić, M. Gotić, A. Turković, A.M. Tonejc, O. Gamulin, J. Molec. Struct. 480–481 (1999) 641.
[26] M. Ivanda, S. Musić, M. Gotić, U.V. Desnica, A.M. Tonejc, T. Bischof, W. Kiefer, Functional Mater. 6 (1999) 530.
[27] L. Sangaletti, L.E. Depero, B. Allieri, F. Pioselli, E. Comini, G. Sberveglieri, M. Zocchi, J. Mater. Res. 13 (1998) 2457.
[28] J. Giuntini, W. Granier, J.V. Zanchetta, A. Taha, J. Mater. Sci. Lett. 9 (1990) 1383.
[29] M. Ocaña, C.J. Serna, Spectrochim. Acta A 47 (1991) 765.
[30] M. Ocaña, C.J. Serna, J.V. Garcia-Ramos, E. Matijević, Solid State Ionics 63–65 (1993) 170.
[31] V.M. Jiménez, A. Caballero, A. Fernandez, J.P. Espinós, M. Ocaña, A.R. González-Elipe, Solid State Ionics 116 (1999) 117.